Journal of Inorganic Biochemistry 194 (2019) 65–73

Contents lists available at ScienceDirect

Journal of Inorganic Biochemistry

journal homepage: www.elsevier.com/locate/jinorgbio

Synthesis, characterization and antimicrobial activity of *N*-acetyl-3-acetyl-5-benzylidene tetramic acid-metal complexes. X-ray analysis and identification of the Cd(II) complex as a potent antifungal agent

Dimitris Matiadis[a,*], Dimitrios Tsironis[a], Valentina Stefanou[a], Alysha G. Elliott[b], Konstantinos Kordatos[c], Georgia Zahariou[d], Nikolaos Ioannidis[d], Vickie McKee[e,f], Angeliki Panagiotopoulou[g], Olga Igglessi-Markopoulou[a], John Markopoulos[h,*]

[a] National Technical University of Athens, School of Chemical Engineering, Laboratory of Organic Chemistry, Zografou Campus, Athens 15773, Greece
[b] The Institute for Molecular Bioscience, The University of Queensland, Qld, Australia
[c] National Technical University of Athens, School of Chemical Engineering, Laboratory of Inorganic and Analytical Chemistry, Zografou Campus, Athens 15773, Greece
[d] Institute of Nanoscience and Nanotechnology, NCSR "Demokritos", Ag. Paraskevi, 15310, Attiki, Greece
[e] School of Chemical Sciences, Dublin City University, Glasnevin, Dublin 9, Ireland
[f] Department of Physics, Chemistry and Pharmacy, University of Southern Denmark, Campusvej 55, 5230 Odense, Denmark
[g] Institute of Biosciences and Applications, NCSR "Demokritos", Ag. Paraskevi, 15310, Attiki, Greece
[h] Laboratory of Inorganic Chemistry, Department of Chemistry, National and Kapodistrian University of Athens, Panepistimiopolis, 15771 Athens, Greece

ARTICLE INFO

Keywords:
Tetramic acid
Pyrrolidine-2,4-dione
Metal complex
Antibacterial activity
Antifungal activity
Crystal structure

ABSTRACT

This study aims at the further expansion of knowledge on the antimicrobial activities of the tetramic acid moiety and the effect of metal complexation. Complexes of the *N*-acetyl-3-acetyl-5-benzylidenetetramic acid with Mn, Co, Ni, Cu, Zn and Cd were synthesized and screened against 5 key ESKAPE pathogens (*Escherichia coli,* methicillin-resistant *Staphylococcus aureus* (MRSA), *Klebsiella pneumoniae, Acinetobacter baumannii* and *Pseudomonas aeruginosa*) and 2 fungi (*Cryptococcus neoformans* and *Candida albicans*). The cadmium complex was found to effectively inhibit the fungus *Cryptococcus neoformans* with minimum inhibitory concentration (MIC) of 8 μg/mL, with no human cell toxicity and hemolytic activity within the tested concentration range. The biologically active tetramic acid-cadmium complex was structurally characterized by single-crystal X-ray analysis. Furthermore, the thermal stability of the ligand and the complexes was investigated along with NMR and EPR studies of the Cd(II) and Co(II) complexes respectively.

1. Introduction

Antibiotic resistance represents one of the biggest threats to global health today [1]. Even though antimicrobials continue to cure deadly diseases, the emerging multi-drug resistant pathogens have become a serious threat to humanity, as this phenomenon combined with the decreasing number of novel drugs may lead to the disastrous scenario of a post-antibiotic era [2].

In particular, fungal pathogens are major causes of morbidity and mortality in immunocompromised patients. Infections from fungi like *Candida albicans* and *Cryptococcus neoformans* are often life-threatening to patients with HIV-AIDS or cancer [3]. Unfortunately, only a limited number of antifungal agents are available due to the fact that fungi are eukaryotic organisms as are their mammalian hosts [4]. Additionally, resistance against most drugs has already been developed [5,6].

Since antibacterial and antifungal drug resistance has been acknowledged as inevitable, new classes of these agents need to be developed. Naturally occurring tetramic acids streptolydigin [7], reutericyclin [8], magnesidin [9] and, more recently vermelhotin [10] have found to possess antibacterial activities [11]. Moreover, potent antifungal natural products of this class or analogues have been identified, such as the aurantosides D, E, F [12], K [13], cryptocin [14], talaroconvolutins [15] and pramanicin [16] (Fig. 1).

These structures have inspired synthetic and medicinal chemists to focus on the tetramic acids and the endless possibilities of derivatizing them in order to reach novel antibiotic compounds [17]. Various structure activity relationship studies on antimicrobial activities have been published, often with impressive results [18–22]. In one of these works [21], it has been shown that some copper(II) tetramic acid complexes exhibit higher activity than their parent compounds.

* Corresponding authors.
E-mail addresses: dmatiadis@gmail.com (D. Matiadis), jmmarko@chem.uoa.gr (J. Markopoulos).

https://doi.org/10.1016/j.jinorgbio.2019.02.008
Received 15 October 2018; Received in revised form 10 February 2019; Accepted 18 February 2019
Available online 21 February 2019
0162-0134/

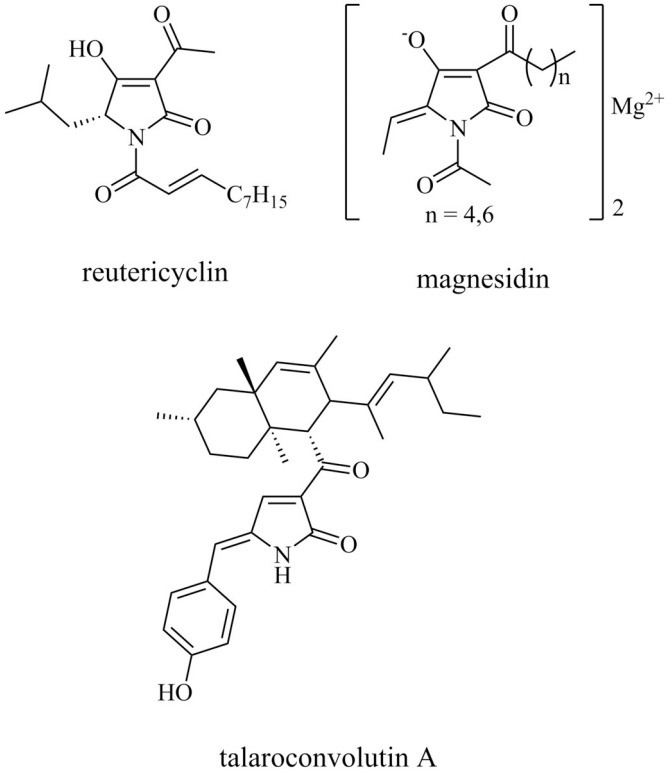

Fig. 1. Structures of antibacterial/antifungal tetramic acids or analogues.

Recently, a series of ampicillin-tetramic acid hybrids and other β-lactam-tetramic acid hybrids were synthesized and evaluated with improved activity against *Pseudomonas aeruginosa* and moderate activity against other bacteria [23,24].

Our research group has contributed significantly to the synthesis and study of five-membered β,β′-tricarbonyl nitrogen [25], oxygen [26] and sulfur heterocycles [27] and their coordination compounds [28]. In particular, we have published a number of studies on five-membered heterocycles bearing an arylidene group at C-5 of the ring [29–32]. Recent studies on similar oxygen and sulfur compounds have reported significant antimicrobial activities [33,34].

The ability of *N*-acetyl-3-acyl-5-arylidene-tetramic (Haabta) to form metal complexes [35–38] that further increases the lipophilicity of these molecules which already contain two lipophilic groups [35] - the acetyl or alkanoyl at C-3 and the arylidene at C-5 - prompted us to investigate their potency as antimicrobial inhibitors.

2. Experimental

2.1. General

All reagents were purchased from Aldrich and Fluka and used without further purification. Dry THF was distilled from Na/Ph_2CO. Melting points were determined with a Gallenkamp MFB-595 melting point apparatus. NMR spectra were recorded with a Bruker Avance 500 MHz spectrometer operating at 500 MHz (^1H) and 125 (^{13}C). Chemical shifts are reported in ppm relative to $CDCl_3$ (^1H: δ = 7.26 ppm) or DMSO-d_6 (^1H: δ = 2.50 ppm, ^{13}C: δ = 39.52 ± 0.06 ppm). *UV* spectra were recorded with a Jasco V-770 spectrophotometer using $CHCl_3$. IR spectra were recorded on a Jasco 4200 Spectrometer using KBr pellets. Thermo-gravimetric analyses were performed with a Mettler-Toledo TGA/SDTA 851e instrument under nitrogen atmosphere at a heating rate of 10 °C/min from room temperature to 900 °C. HRMS spectra were recorded on UHPLC LC-MSn Orbitrap Velos-Thermo instrument in the Institute of Biology, Medicinal Chemistry and Biotechnology of the National Hellenic Research Foundation.

EPR measurements were obtained with a Bruker ER-200D spectrometer (for X-band) interfaced to a personal computer, equipped with an Oxford ESR-900 cryostat, an Anritsu MF79A frequency counter, an SR830 digital lock-in amplifier by Stanford Research, and a Bruker 035 M NMR gaussmeter. The perpendicular 4102ST (for X-band) and ER5106QT (for Q-band) cavities were used, and the microwave frequencies were 9.41 GHz and 34 GHz for X-band and Q-band, respectively.

X-ray data were collected at 100(2)K on a Synergy, Dualflex, AtlasS2 diffractometer using CuKα radiation (λ = 1.54184 Å) and the *CrysAlis PRO* 1.171.39.27b suite [39]. Using SHELXLE [40] the structure was solved by dual space methods (SHELXT [41]) and refined on F^2 using all the reflections (SHELXL-2017/1 [42]). All the non-hydrogen atoms were refined using anisotropic atomic displacement parameters and hydrogen atoms bonded to carbon were inserted at calculated positions using a riding model; the hydrogen atoms of the water molecule were located from difference maps and refined with their thermal parameters riding on the carrier oxygen atom. The structure was refined as a 2-component twin. Component 2 rotated by 179.9° around [0.67–0.73 0.14] (reciprocal) or [0.71–0.71 -0.00] (direct) R1 = 0.0297 for 2920 unique reflections after merging for Fourier. Crystal data, data collection and structure refinement details are summarized in Table 3. CCDC 1871745 contains the supplementary crystallographic data for this paper. These data can be obtained free of charge from The Cambridge Crystallographic Data Centre via www.ccdc.cam.ac.uk/data_request/cif.

The ligand Haabta **(1)** was synthesized according to our previously described method [29] without any modification.

2.2. Synthesis of the metal complexes **(2–7)**

To a solution of the Haabta **1** (135 mg, 0.50 mmol) in the minimum possible amount of methanol was added the appropriate metal (II) acetate* (0.25 mmol) dissolved in the minimum possible amount of methanol. For the synthesis of **4** and **7**, ethanol was used instead of methanol. The resulting solution was refluxed for 2 h, left to cool at rt. and then overnight at 0–4 °C. The precipitate was filtered and washed with EtOH and dried under vacuum and P_2O_5.

*The metal acetates we used are: $Ni(CH_3COO)_2{\cdot}4H_2O$, $Co(CH_3COO)_2{\cdot}4H_2O$, $Zn(CH_3COO)_2{\cdot}2H_2O$, $Mn(CH_3COO)_2{\cdot}4H_2O$, $Cd(CH_3COO)_2{\cdot}2H_2O$ and $Cu(CH_3COO)_2{\cdot}H_2O$.

2.2.1. *[Ni(aabta)$_2$(H$_2$O)$_2$]* **(2)**

Yield 117 mg (74%), light green solid, mp 285 °C (dec.), ν_{max}/cm^{-1}: 3196(s), 1737(s), 1659(s), 1605(s), 1468(s), 1375(s), 443(m), HRMS [M^+ - $2H_2O$]: calcd for $C_{30}H_{24}N_2NiO_8$ 599.0964; found 599.0958.

2.2.2. *[Co(aabta)$_2$(H$_2$O)$_2$]* **(3)**

Yield 132 mg (84%), beige solid, mp 245 °C (dec.), ν_{max}/cm^{-1}: 3454(s), 1711(s), 1680(m), 1604(s), 1462(s), 1305(m), 605(m), HRMS [M^+ - $2H_2O$]: calcd for $C_{30}H_{24}N_2CoO_8$ 600.0943; found 600.0955.

2.2.3. *[Zn(aabta)$_2$(EtOH)$_2$]* **(4)** *[29]*

Yield 119 mg (68%), off-white solid, mp 218–220 °C, ν_{max}/cm^{-1}: 3222(m), 1736(m), 1691(m), 1606(s), 1468(s), 1374(m), 471(w).

2.2.4. *[Mn(aabta)$_2$(MeOH)$_2$]* **(5)**

Yield 111 mg (67%), bright yellow solid, mp 228 °C (dec.), ν_{max}/cm^{-1}: 3425(s), 1717(m), 1663(m), 1607(s), 1463(s), 1372(m), 532(w), HRMS [M^+ - 2MeOH]: calcd for $C_{30}H_{24}N_2MnO_8$ 596.0991; found 596.0994.

2.2.5. *[Cd(aabta)$_2$(H$_2$O)$_2$]* **(6)**

Yield 129 mg (75%), ivory white solid, mp 219 °C (dec.), $\nu_{max}/$

cm^{-1}: 3419(m), 1731(m), 1663(m), 1603(s), 1454(s), 1371(m), 531(w), δ_H (500 MHz; DMSO-d_6) 2.37 (6H, s, CH_3CON), 2.47 (6H, s, CH_3COC-3), 6.77 (2H, s, CH=) and 7.16–7.32 (10H, m, Ph), δ_H (500 MHz; $CDCl_3$) 1.71 (4H, br, coord. H_2O), 2.30 (6H, s, CH_3CON), 2.54 (6H, s, CH_3COC-3), 7.19 (2H, s, CH=) and 7.26–7.34 (10H, m, Ph), δ_C (125 MHz; DMSO-d_6) 26.4 (CH_3COC-3), 28.7 (CH_3CON), 100.1 (C-3), 114.6 (PhCH=), 127.6, 129.9, 131.1 (Ph), 135.4 (C-5), 167.8 (C-2), 169.9 (CH_3CON), 183.1 (C-4), 197.1 (CH_3COC-3). HRMS [M^+ - $2H_2O$]: calcd for $C_{30}H_{24}N_2CdO_8$ 655.0644; found 655.0654.

2.2.6. [Cu(aabta)$_2$(EtOH)$_2$] (7) [29]

Yield 124 mg (74%), green solid, mp 172 °C (dec.), ν_{max}/cm^{-1}: 3665, 3564, 3199(s), 1736(m), 1694(s), 1588(s), 1489(s), 1374(m), 465(w).

2.3. Biological methods

Minimum Inhibitory Concentration bacterial and fungal assays, cytotoxicity assays and hemolysis assays were conducted as previously described [43] with the exception that compounds in this study were plated prior to cell addition in the cytotoxicity assay. Detailed methods are described as follows.

2.3.1. Sample preparation for preliminary single-point screening and minimum inhibition concentration assays (MIC), cytotoxicity and hemolysis assays.

For single-point preliminary inhibitory assays, solutions of the samples were prepared in DMSO and water to a final testing concentration of 32 μg/mL, in 384-well, non-binding surface plate (NBS) for each bacterial/fungal strain, and in duplicate (n = 2), and keeping the final DMSO concentration to a maximum of 1% DMSO. All the sample-preparation where done using liquid handling robots. Colistin and vancomycin were used as positive bacterial inhibitor standards for Gram-negative and Gram-positive bacteria, respectively. Fluconazole was used as a positive fungal inhibitor standard for *C. albicans* and *C. neoformans*.

The compound **6**, which was flagged as active in the preliminary screening was then serially diluted 1:2 fold for 8 times. Each sample concentration was prepared in 384-well plates, non-binding surface plate (NBS; Corning 3640) for each bacterial/fungal strain, tissue-culture treated (TC-treated; Corning 3712/3764) black for mammalian cell types and polypropylene 384-well (PP; Corning 3657) for haemolysis assays, all in duplicate (n = 2), and keeping the final DMSO concentration to a maximum of 0.5%.

2.3.2. Antimicrobial assay

All bacteria were cultured in Cation-adjusted Mueller Hinton broth (**CAMHB**) at 37 °C overnight. A sample of each culture was then diluted 40-fold in fresh broth and incubated at 37 °C for 1.5–3 h. The resultant mid-log phase cultures were diluted (Colony Forming Units - CFU/mL measured by OD_{600}), then added to each well of the compound containing plates, giving a cell density of 5×10^5 CFU/mL and a total volume of 50 μL. All the plates were covered and incubated at 37 °C for 18 h without shaking.

Inhibition of bacterial growth was determined measuring absorbance at 600 nm (OD_{600}), using a Tecan M1000 Pro monochromator plate reader. The percentage of growth inhibition was calculated for each well, using the negative control (media only) and positive control (bacteria without inhibitors) on the same plate as references. The significance of the inhibition values was determined by modified Z-scores, calculated using the median and Median Absolute Deviation (MAD) of the samples (no controls) on the same plate.

For single-point preliminary screening, samples with inhibition > 80% and Z-Score above 2.5 for either replicate (n = 2 on different plates) when tested at 32 μg/mL were classed as actives. Samples with inhibition values between 50 and 80% and Z-Score above 2.5 for either replicate (n = 2 on different plates) were classed as partial actives.

The minimum inhibitory concentration (MIC) of **6** was determined as the lowest concentration at which the growth was fully inhibited in the dose response assay (0.25–32 μg/mL), defined by an inhibition ≥80%. 80% value is used to allow for the fluctuation of growth that is typically 10–20% for any given bacterial or fungi assay.

2.3.3. Antifungal assay

Fungi strains were cultured for 3 days on Yeast Extract-Peptone Dextrose (YPD) agar at 30 °C. A yeast suspension of 1×10^6 to 5×10^6 CFU/mL (as determined by OD_{530}) was prepared from five colonies. The suspension was subsequently diluted and added to each well of the compound-containing plates giving a final cell density of fungi suspension of 2.5×10^3 CFU/mL and a total volume of 50 μL. All plates were covered and incubated at 35 °C for 24 h without shaking.

Growth inhibition of *C. albicans* was determined measuring absorbance at 530 nm (OD_{530}), while the growth inhibition of *C. neoformans* was determined measuring the difference in absorbance between 600 and 570 nm ($OD_{600-570}$), after the addition of resazurin (0.001% final concentration) and incubation at 35 °C for additional 2 h. The absorbance was measured using a Biotek Synergy HTX plate reader. The percentage of growth inhibition was calculated for each well, using the negative control (media only) and positive control (fungi without inhibitors) on the same plate. The significance of the inhibition values was determined by modified Z-scores, calculated using the median and MAD of the samples (no controls) on the same plate.

For single-point preliminary screening, samples with inhibition > 80% and Z-Score above 2.5 for either replicate (n = 2 on different plates) when tested at 32 μg/mL were classed as actives. Samples with inhibition values between 50 and 80% and Z-Score above 2.5 for either replicate (n = 2 on different plates) were classed as partial actives.

The MIC of the active compound **6** was determined as the lowest concentration at which the growth was fully inhibited in the dose response assay (0.25–32 μg/mL), defined by an inhibition ≥80% for *C. albicans* and an inhibition ≥70% for *C. neoformans*. Due to a higher variance in growth and inhibition, a lower threshold was applied to the data for *C. neoformans*.

2.3.4. Cytotoxicity assay

Cytotoxicity to human embryonic kidney cells (HEK293) was determined using the resazurin assay as previously described [44,45]. Briefly, HEK293 cells were counted manually in a Neubauer haemocytometer and then plated in the 384-well plates containing the compound **6** at an 8-point dose response (0.25–32 μg/mL) to give a density of 5000 cells/well in a final volume of 50 μL Dulbecco's Modified Eagle Medium (**DMEM)** supplemented with 10% Fetal Bovine Serum **(FBS)** was used as growth media and the cells were incubated together with the compounds for 20 h at 37 °C in 5% CO_2.

Cytotoxicity (or cell viability) was measured by fluorescence, ex: 560/10 nm, em: 590/10 nm ($F_{560/590}$), after addition of 5 μL of 25 μg/mL resazurin (2.3 μg/mL final concentration) and after incubation for further 3 h at 37 °C in 5% CO_2. The fluorescence intensity was measured using a Tecan M1000 Pro monochromator plate reader, using automatic gain calculation.

CC_{50} (concentration at 50% cytotoxicity) were calculated by curve fitting the inhibition values vs. log(concentration) using a sigmoidal dose-response function, with variable fitting values for bottom, top and slope. In addition, the maximal percentage of cytotoxicity is reported as D_{Max}, indicating any compounds with partial cytotoxicity.

The curve fitting was implemented using Pipeline Pilot's dose-response component, resulting in similar values to curve fitting tools such as GraphPad's Prism and IDBS's XlFit. Any value with > indicate sample with no activity (low D_{Max} value) or samples with CC_{50} values above the maximum tested concentration (higher D_{Max} value).

Cytotoxic samples were classified by $CC_{50} \leq 32$ μg/mL in either replicate (n = 2 on different plates).

2.3.5. Hemolysis assay

Human whole blood was washed three times with 3 volumes of 0.9% NaCl and then resuspended in same to a concentration of 0.5×10^8 cells/mL, as determined by manual cell count in a Neubauer haemocytometer and used for hemolysis assay as previously described [46]. Briefly, the washed cells were then added to the 384-well compound-containing plates at an 8-point dose response (0.25–32 μg/mL) for a final volume of 50 μL. After a 10 min shake on a plate shaker the plates were then incubated for 1 h at 37 °C. After incubation, the plates were centrifuged at 1000*g* for 10 min to pellet cells and debris, 25 μL of the supernatant was then transferred to a polystyrene 384-well assay plate.

Hemolysis was determined by measuring the supernatant absorbance at 405 mm (OD_{405}). The absorbance was measured using a Tecan M1000 Pro monochromator plate reader.

HC_{10} and HC_{50} (concentration at 10% and 50% hemolysis, respectively) were calculated by curve fitting the inhibition values vs. log (concentration) using a sigmoidal dose-response function with variable fitting values for top, bottom and slope. In addition, the maximal percentage of hemolysis is reported as D_{Max}, indicating any compounds with partial hemolysis.

The curve fitting was implemented using Pipeline Pilot's dose-response component, resulting in similar values to curve fitting tools such as GraphPad's Prism and IDBS's XlFit. Any value with > indicate sample with no activity (low D_{Max} value) or samples with HC_{10} values above the maximum tested concentration (higher D_{Max} value).

Hemolysis samples were classified by $HC_{10} \leq 32$ μg/mL in either replicate (n = 2 on different plates). In addition, samples were flagged as partial hemolytic if $D_{Max} \geq 50\%$, even with HC_{10} > the maximum tested concentration.

3. Results and discussion

3.1. Synthesis of the complexes

N-Acetyl-3-acetyl-5-benzylidene tetramic acid **1** (Haabta) was synthesized according to our previously published method from commercially available 4-benzylidene-2-methyl-5(4H)-oxazolone and ethyl acetoacetate [29]. The complexes were prepared by addition of the appropriate metal acetate dissolved in the minimum quantity of methanol or ethanol to a hot methanolic or ethanolic solution of the tetramic acid, followed by reflux for 2 h (Scheme 1). The metal complexes were precipitated as powder solids. After completion of precipitation at room temperature, the mixture was filtered and washed with methanol or ethanol. The complexes were insoluble to most solvents except chloroform, acetone and DMSO.

3.2. Single crystal X-ray diffraction studies

The structure of $[Cd(aabta)_2(H_2O)_2]$ **6** is shown in Fig. 2. The cadmium ion lies on a center of symmetry and is six coordinate. Two monodeprotonated, bidentate aabta ligands are coordinated through the deprotonated alcohol (O3) and a neighbouring carboxy group (O2); two water molecules complete the coordination sphere. As with the published $[Zn(aabta)_2(EtOH)_2]$ **4** [29], the only slightly unusual bond length is the short C5 - O3 (1.253(4) Å), suggesting some delocalisation (Table 1). The coordinated water molecule makes hydrogen bonds (Table 2) to two neighbouring molecules; to O1 (2.768(4) Å under symmetry operation −x + 2, −y + 1, −z + 1) and to O4 (2.810 (4)Å under symmetry operation −x + 1, −y + 1, −z + 1) (Fig. 3). This results in hydrogen-bonded 2D sheets lying perpendicular to the c axis, with the phenyl substituents lying on either side of the plane. There are edge-to-edge π-interactions between chains, involving the phenyl and alkene side chain (Fig. 4).

Symmetry codes: (ii) $-x + 2, -y + 2, -z + 1$; (iii) $-x + 2, -y + 1, -z + 1$; (iv) $-x + 1, -y + 1, -z + 1$.

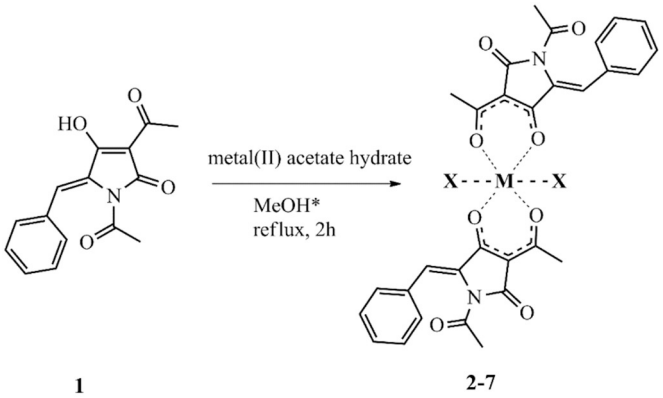

1 **2-7**

Compound	M	X
2	Ni	H_2O
3	Co	H_2O
4	Zn	EtOH
5	Mn	MeOH
6	Cd	H_2O
7	Cu	EtOH

Scheme 1. Synthesis of novel (**2**, **3**, **5**, **6**) and known (**4**, **7**) complexes of Haabta. *Ethanol was used for the synthesis of **4**, **7**.

3.3. NMR spectra analysis

The metal-oxygen bond formation is confirmed by the ^{1}H NMR spectrum in DMSO-d_6 of the Cd(II) coordination compound, since the signal of the enolic proton of the ligand is absent. The two coordinated water molecules appear in the $CDCl_3$ spectrum of the complex. The overall pattern of the spectrum is in accordance with the previously reported NMR spectra of **1** and **4**. Unsurprisingly, the protons appeared high-field shifted in comparison with the free ligand [29,37]. The active complex **6** proved to be stable in DMSO and in the aqueous medium of the biological tests (1% DMSO in water) up to 72 h given its unchanged ^{1}H NMR spectra. Additionally, the ligands remained firmly bound to the cadmium by the 3-acetyl and 4-enolic oxygens as evidenced from the ^{13}C, ^{1}H HMBC NMR spectrum (298 K) of compound **6** in DMSO-d_6 taken over 18 h. This experiment shows the stability and the coordination mode of the molecule. No new heteronuclear correlation observed in the HMBC spectrum in the region where the three carbonyl carbons appear at 167.8, 169.9, and 197.1 and the enolic carbon at 183.1 ppm that correspond to C-2, CH_3CON-, CH_3COC-3 and C-4 carbons of the complex respectively.

3.4. Thermogravimetric analysis (TGA)

The proposed structures where further supported by the thermogravimetric analyses. Thermogravimetric and Differential Thermal Gravimetric (TG/DTG) analyses of the ligand and the metal complexes were carried out from room temperature to 900 under a nitrogen atmosphere. The data are summarized in Table 4 and representative graphs of the cadmium (II) complex **6** and the ligand **1** are given in Fig. 5. The TG/DTG curves of the ligand **1** show no mass loss up to 184 °C, indicating the high thermal stability of the molecule. From 184 to 414 °C the molecule loses 61.11% (calcd. 61.26%) of its mass, accompanied by a peak at 263 °C, which is assigned to the removal of the phenyl group and the two acetyl groups.

The TG/DTG curves of the metal (II) complexes show in general a three step decomposition. The first step may be attributed to the removal of the solvent molecules. In the case of complexes **2** and **3**, the peak temperatures correspond to weakly coordinated water molecules, whereas the peak temperatures of the first step of the complexes **5**, **6**

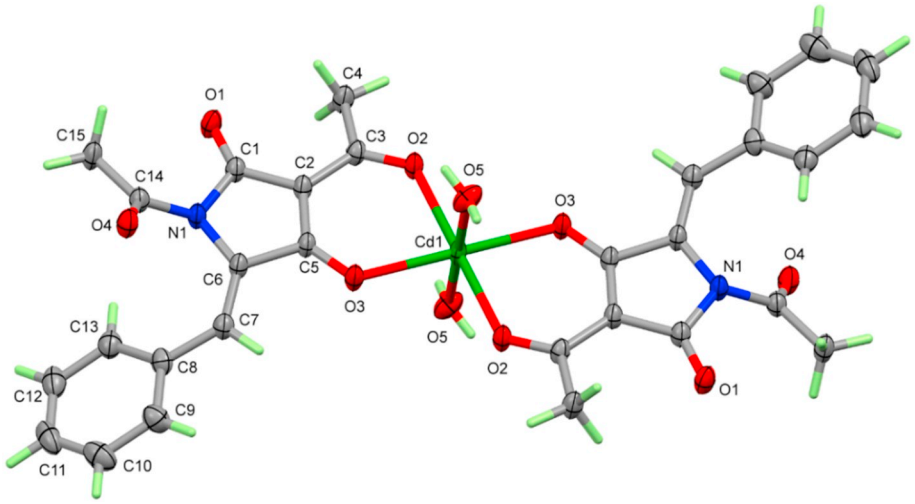

Fig. 2. Molecular structure of **6**. Non-hydrogen atoms are drawn with 50% probability ellipsoids.

Table 1
Selected geometric parameters (Å, °) for **6**.

Cd1−−O3	2.246 (2)	O3−Cd1−O2	83.96 (8)
Cd1−O2	2.254 (2)	$O2^{i}$−Cd1−O2	180.0
Cd1−O5	2.292 (3)	O3−Cd1−O5	91.28 (10)
O2−C3	1.251 (4)	O2−Cd1−O5	93.82 (9)
O3−C5	1.254 (4)	C3−O2−Cd1	130.7 (2)
$O3^{i}$−Cd1−O3	180.0	C5−O3−Cd1	124.1 (2)
$O3^{i}$−Cd1−O2	96.04 (8)		

Table 2
Hydrogen-bond geometry (Å, °) for **6**.

D−H···*A*	*D*−H	H···*A*	*D*···*A*	*D*−H···*A*
C4−H4*C*···$O2^{ii}$	0.98	2.62	3.502 (4)	150
C15−H15*A*···$O2^{iii}$	0.98	2.59	3.386 (5)	139
O5−H5*B*···$O1^{iii}$	0.74 (6)	2.05 (6)	2.767 (4)	164 (6)
O5−H5*A*···$O4^{iv}$	0.84 (6)	1.98 (6)	2.809 (4)	170 (5)

Symmetry codes: (ii) $-x+2, -y+2, -z+1$; (iii) $-x+2, -y+1, -z+1$; (iv) $-x+1, -y+1, -z+1$.

and **7** correspond to strongly coordinated methanol or water molecules. Noteworthy, the complex **4** loses one ethanol molecule at relatively low temperature (78–149 °C). The second step of decomposition (~300 °C) is generally attributed to the loss of the non-coordinated acetyl group of the molecule. In the third step, the removal of the phenyl group is observed at high temperatures (~400 °C), probably due to the intermolecular π-interactions, which stabilize the group. Further heating resulted in continuous loss of mass, indicating the decomposition of the molecules, which is not complete up to 900 or 1000 °C due to the presence of metal oxides and residual carbon material.

3.5. Electronic spectra analysis

The UV–Vis spectra of the ligand and the Mn(II), Co(II), Ni(II) and Cd(II) complexes were recorded in $CHCl_3$ in 245–800 nm range in ambient temperature.

The presence of a wide range of bands is due to both $\pi \rightarrow \pi^*$, $n \rightarrow \pi^*$ and d-d transitions and also due to charge transfer transitions arising from π electron interactions between the ligand and the metals [47,48] (Tables 5, 6).

3.5.1. Ni(II) complex 2

The absorption spectra of the d^8 Ni(II) complex displays two d-d transitions at 581 nm ($\varepsilon = 39\ M^{-1}{\cdot}cm^{-1}$) and 491 nm ($\varepsilon = 31.7\ M^{-1}{\cdot}cm^{-1}$) which correspond to $^3A_{2g} \rightarrow {}^3T_{1g}$ (F) and $^3A_{2g} \rightarrow {}^3T_{1g}$ (P) transitions [49].

3.5.2. Co(II) complex 3

The electronic spectrum of the d^7 Co(II) complex showed two bands at 530 nm ($\varepsilon = 184\ M^{-1}{\cdot}cm^{-1}$) and 429 cm-1 ($\varepsilon = 1796\ M^{-1}{\cdot}cm^{-1}$) assigned to the transitions $^4T_{1g}$ (F) → $^4A_{2g}$ (F) and $^4T_{1g}$ (F) → $^4T_{1g}$ (P) respectively, suggesting an octahedral geometry around the Co(II) ion [50].

3.5.3. Mn(II) complex 5

The analysis of d-d bands plays an important role in studying the interactions between central ions and ligands in complexes. The octahedral high-spin d^5 complexes have no excited states of the same spin multiplicity [48] as the ground state. The bands that are observed as the consequence of spin-forbidden transitions are typically weak [51]. The Mn(II) complex exhibit three absorption bands in the range of 529 nm ($\varepsilon = 278\ M^{-1}{\cdot}cm^{-1}$), 489 ($\varepsilon = 298\ M^{-1}{\cdot}cm^{-1}$) and 454 ($\varepsilon = 385\ M^{-1}{\cdot}cm^{-1}$) assigned to the transitions $^6A_{1g} \rightarrow {}^4T_{1g}$ (4G), $^6A_{1g} \rightarrow {}^4T_{2g}$ (4G) and $^6A_{1g} \rightarrow {}^4A_{1g}$ (4G), ^4E_g (4E) respectively.

3.5.4. Racah parameters

The Racah parameters of the above complexes were calculated from the Tanabe-Sugano diagrams (Table 7). From Table 7, the interelectronic repulsion parameter (B′) suggests a considerable orbital overlap and delocalization of electrons of the metal ions. In addition, the nephelauxetic ratio β of the complexes indicates an appreciable covalent character of the metal-ligand "σ" bond [48,50,52].

3.6. EPR spectra of the Co(II) compound 3

The EPR spectra of the Co(II) compound **3** at X-band and at Q-band are shown in Fig. 6.

Both of the spectra present similar features of a S = 3/2, with a rhombic g-anisotropy with g_{eff} values of 2.07, 2.72, 7.5, which are better resolved in the Q-band spectrum (Panel B). This observation indicates a ground state with a high-spin configuration of the d^7 Co(II) ion, with an anisotropic ligand-environment [53]. Additionally, the hyperfine structure that is revealed at X-band spectrum (Panel A) is assigned to the hyperfine interaction of the S = 3/2 with $I = 7/2$ of the ^{59}Co nucleus. The EPR signals at both X- and Q-band originate from the transition within either the $|\pm 1/2>$, or the $|\pm 3/2>$ Kramer's doublet. The absence of any additional EPR signal assigned to an inter-doublet transition indicates that the energy difference between the Kramer's doublets is much higher than ~1.2 cm^{-1} (=microwave

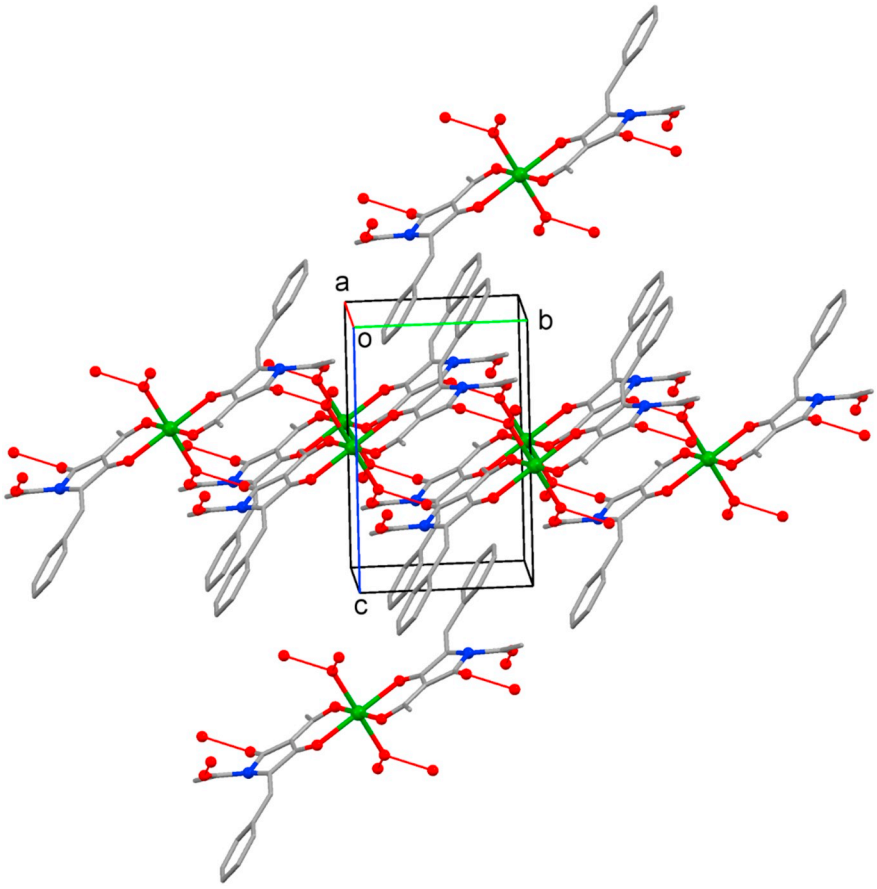

Fig. 3. Unit cell packing diagram for 6. Hydrogen atoms omitted for clarity. Hydrogen bonds are shown as red dashed lines.

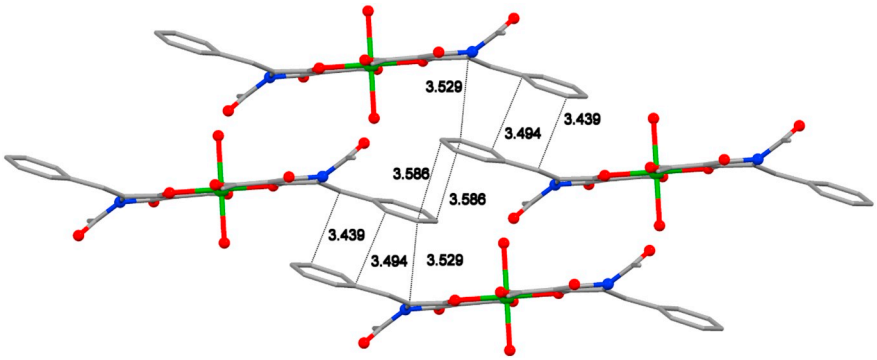

Fig. 4. Intermolecular edge-to-edge π-interactions. Hydrogen atoms are omitted for clarity.

energy at Q-band).

3.7. Biological evaluation

3.7.1. In vitro antibacterial and antifungal activity

In order to determine the potential antimicrobial activity of the compounds 1–7, single point concentration (32 μg/mL; n = 2) broth antimicrobial screening against 5 key ESKAPE pathogens *Escherichia coli*, *Staphylococcus aureus* (MRSA), *Klebsiella pneumoniae*, *Acinetobacter baumannii* and *P. aeruginosa*, and 2 fungi *C. neoformans* and *C. albicans* was undertaken. When tested at 32 μg/mL all compounds were deemed inactive, except for compound **6** which showed partial activity against *S. aureus* (MRSA), i.e. 50–80% growth inhibition, and full inhibition against *C. neoformans* with 100% inhibition at 32 μg/mL, compared to growth and media controls. To confirm the activity of compound **6** an 8-point dose response (0.25 μg/mL – 32 μg/mL) antimicrobial activity assay was performed in duplicate, and activity expressed as minimum inhibitory concentrations (MIC). These assays were performed on both the target resulting from the primary screening results, *C. neoformans* as well as the full panel of bacteria/fungi for a uniform directly comparable data set for this lead candidate compound (Table 8). Appropriate positive inhibitory antibiotic controls were included for each strain testes and data provided in the supplementary information.

3.7.2. Cytotoxicity and red blood cells hemolysis

To investigate the specificity of compound **6** as a potential antifungal, it was assayed against a mammalian cell line and human red blood cells (RBCs) to determine general cell toxicity.

Although compound **6** shows inhibitory activity against the fungi *C. neoformans* (MIC of 8 μg/mL), it was found to be non-hemolytic in a dose response (0.25 μg/mL – 32 μg/mL) hemolysis assay with HC_{50} > 32 μg/mL (Table 8). The hemolytic activity is used as a

Table 3
Crystal data and structure refinement for compound **6**.

Empirical formula	$C_{30}H_{28}CdN_2O_{10}$
Formula weight	688.94
Temperature/K	100.00(10)
Crystal system	triclinic
Space group	*P*
a/Å	8.0252(4)
b/Å	8.2368(4)
c/Å	12.0385(7)
α/°	81.343(4)
β/°	76.553(5)
γ/°	65.610(5)
Volume/Å^3	703.55(7)
Z	1
ρ_{calc}g/cm^3	1.626
μ/mm^{-1}	6.769
F(000)	350.0
Crystal size/mm^3	0.228 × 0.052 × 0.013
Radiation	Cu Kα (λ = 1.54184)
2Θ range for data collection/°	11.8272 to 153.438
Index ranges	$-10 \le h \le 10$, $-9 \le k \le 9$, $-15 \le l \le 14$
Reflections collected	26,787
Independent reflections	5753 [R_{int} = 0.0580]
Data/restraints/parameters	5753/0/205
Goodness-of-fit on F^2	1.010
Final R indexes [$I \ge 2\sigma$ (I)]	R_1 = 0.0361, wR_2 = 0.0930
Final R indexes [all data]	R_1 = 0.0378, wR_2 = 0.0940
Largest diff. peak/hole/e Å^{-3}	1.17/−0.84

Table 4
Thermal analysis data including temperature range, DT peak, weight loss and proposed segment.

Compound	Temp. range (°C)	Peak temp. (°C)	Proposed segment	Weight loss (%)	
				Calc.	Found
Haabta **(1)**[a]	184–414	270	C_6H_5, 2xC_2H_3O	61.26	61.11
Ni(aabta)$_2$(H_2O)$_2$ **(2)**	131–202	158	2xH_2O	6.42	5.67
	219–378	299	2xC_2H_3O	13.55	13.02
	378–520	405, 458	2xC_6H_5	24.28	28.18
Co(aabta)$_2$(H_2O)$_2$ **(3)**	122–175	140	2xH_2O	5.67	5.48
	219–334	263	2xC_2H_3O	13.53	11.49
	334–520	422, 440, 484	2xC_6H_5	24.25	27.58
Zn(aabta)$_2$(EtOH)$_2$ **(4)**	78–149	122	EtOH	6.60	5.39
	210–387	237, 290	EtOH, 2xC_2H_3O	18.93	20.23
	387–608	476	2xC_6H_5	22.09	20.53
Mn(aabta)$_2$(MeOH)$_2$ **(5)**	210–310	255	2xMeOH	9.70	8.66
	310–407	378	2xC_2H_3O	13.04	11.28
	407–570	461	2xC_6H_5	23.35	19.38
Cd(aabta)$_2$(H_2O)$_2$ **(6)**	184–298	255	2xH_2O	5.23	5.27
	298–387	360	2xC_2H_3O	12.49	9.81
	387–546	430	2xC_6H_5	22.38	21.07
Cu(aabta)$_2$(EtOH)$_2$ **(7)**	184–290	263	2xMeOH	9.59	12.89
	290–449	361	2xC_2H_3O, 2xC_6H_5	35.96	39.68

[a] In the case of the ligand **1**, the two acetyl groups are removed, whereas in the complexes only one acetyl group per ligand is removed; presumably the non-coordinated one.

Table 5
Wavenumbers in nm.

Ligand	Ni(II) complex **2**	Co(II) complex **3**	Mn(II) complex **5**	Cd(II) complex **6**
289	268	261	264	257
349	326	328	327	334

Table 6
Wavenumbers in nm.

Ni(II) complex **2**	Co(II) complex **3**	Mn(II) complex **5**
491	429	454
581	530	489
		529

Table 7
Racah parameters for Ni(II), Co(II) and Mn(II) complexes.

Compound	Δ_o (cm^{-1})	B′	*β*	*β*%
Ni(II) complex **2**	5736	956	0,88	12
Co(II) complex **3**	13,050	840	0,86	14
Mn(II) complex **5**	3917	702	0,81	19

Table 8
Antimicrobial activity against bacteria and fungi as Minimum Inhibitory Concentration (MIC), cytotoxicity (CC_{50}) and hemolytic activity (HC_{50}) of Cd(aabta)$_2$(H_2O)$_2$ **(6)**.

MIC	μg/mL
E. coli ATCC 25922	> 32
K. pneumoniae ATCC 700603 (MDR; ESBL)	> 32
A. baumannii ATCC 19606	> 32
P. aeruginosa ATCC 27853	> 32
S. aureus ATCC 43300 (MRSA)	> 32
C. albicans ATCC 90028	> 32
C. neoformans H99; ATCC 208821	8
Cytotoxicity CC_{50}	
HEK293 (human kidney cell) ATCC CRL-1573	> 32
Hemolysis HC_{50}	
RBC (human red blood cells)	> 32

MDR, multi-drug resistant; ESBL, extended spectrum ß-lactamase; MRSA, Methicillin resistant *S. aureus*.

measure of general cell toxicity and a model for human cells because the red blood cells are considered very fragile. The cytotoxicity of **6** as a growth inhibitor of human embryonic kidney cells (HEK293) was also determined by a dose response (0.25 μg/mL – 32 μg/mL) cell viability assay, and found non-toxic up to the highest tested concentration of 32 μg/mL, i.e. CC_{50} deemed > 32 μg/mL. These results are encouraging, showing ≥4-fold specificity of antifungal activity over general cell toxicity as, in general, antifungal therapeutics are generally toxic. In contrast, when cadmium(II) acetate dihydrate was evaluated for comparison purposes with the active compound **6**, it was found, as expected [54,55], to show high antifungal activity (MIC = 2 μg/mL) associated with high toxicity against human cells (CC50 = 9.6 μg/mL). Therefore, development of drugs that target fungi without affecting human cells is a real challenge and compound **6** shows great potential for further investigation to develop an antifungal agent.

4. Conclusion

We conducted the synthesis, structural determination and evaluation of antimicrobial activities of a group of metal (II) complexes with the *N*-acetyl-3-acetyl-5-benzylidenetetramic acid as a model compound for these tetramic acids with an extended conjugation system. All the compounds are soluble in DMSO. Compound **6** exhibited moderate inhibition of *C. neoformans*. The Cd (II) complex was found to have nonhemolytic and nontoxic antifungal activity. The structure and the intermolecular interactions of the bioactive compound 6 have been investigated by single crystal X-ray crystallography. The EPR spectra of the Co (II) compound reveals a high-spin configuration of the Co(II) ion, with a rhombic g-anisotropy. We are now investigating the effect of structural modification of this class of heterocyclic compounds at

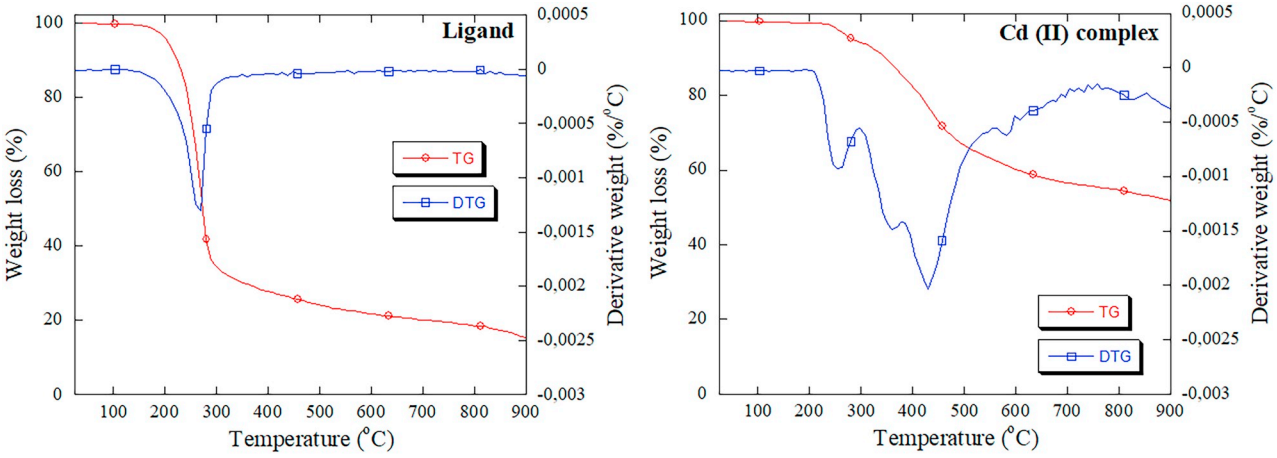

Fig. 5. TG/DTG thermodiagrams of ligand **1** (left) and Cd (II) complex **6** (right), respectively.

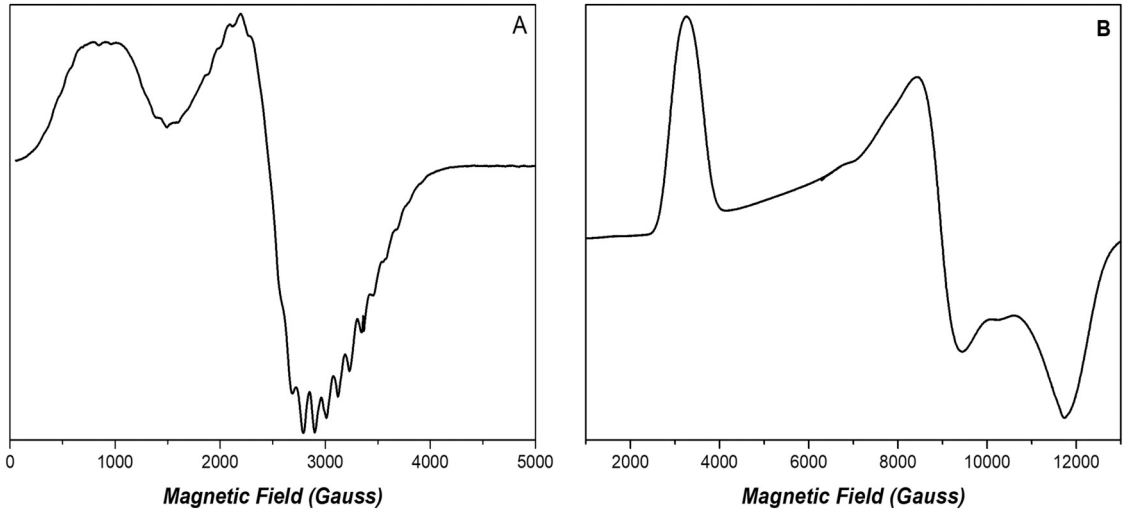

Fig. 6. EPR spectra of the Co(II) compound **3** at X-band (Panel A) and Q-band (Panel B). Experimental Conditions: Temperature, 14 K; Microwave Power, 32 mW; Modulation Amplitude, 10 Gp.p.; Microwave Frequency, 9.41 GHz (Panel A) and 34 GHz (Panel B).

selected sites of the molecule on the antimicrobial activities. This structure-activity relationship study will provide us helpful data to our efforts to identify a nontoxic potent antifungal or antibacterial as a lead compound.

Acknowledgements

Antimicrobial and mammalian cell toxicity screening was performed by CO-ADD (The Community for Open Antimicrobial Drug Discovery) [56], funded by the Wellcome Trust (UK) and The University of Queensland (Australia).

The authors acknowledge Dr. Yiannis Sanakis for the helpful discussions.

GZ and NI acknowledge support of this work by the project MIS 5002567, implemented under the "Action for the Strategic Development on the Research and Technological Sector", funded by the Operational Programme "Competitiveness, Entrepreneurship and Innovation" (NSRF 2014-2020) and co-financed by Greece and the European Union (European Regional Development Fund).

DM would like to thank the Greek State Scholarship Foundation and SIEMENS for an IKY Fellowship of Excellence for Postdoctoral Studies in Greece – SIEMENS Program.

*V*McK acknowledges funding from the Carlsberg Foundation grant CF15-0675 for the X-ray diffractometer and the University of Southern Denmark/Danish Council for Independent Research|Natural Sciences (grant 12-124985) for a visiting professorship.

Appendix A. Supplementary data

Supplementary data to this article can be found online at https://doi.org/10.1016/j.jinorgbio.2019.02.008.

References

[1] World Health Organization. Antimicrobial resistance: global report on surveillance. apps.who.int/iris/bitstream/10665/112642/1/9789241564748_eng.pdf. (Accessed 14 January 2018).
[2] A.J. Alanis, Arch. Med. Res. 36 (2005) 697–705.
[3] T.J. Walsh, A.H. Groll, Transpl. Infect. Dis. 1 (1999) 247–261.
[4] A. Srinivasan, J.L. Lopez-Ribot, A.K. Ramasubramanian, Drug Discov. Today Technol. 11 (2014) 65–71.
[5] M.M. Canuto, F.G. Rodero, Lancet Infect. Dis. 2 (2002) 550–563.
[6] D.S. Perlin, Drug Resist. Updat. 10 (2007) 121–130.
[7] C. Deboer, A. Dietz, G.M. Savage, W.S. Silver, Antibiot. Annu. 3 (1955) 886–892.
[8] A. Hölzen, M.G. Gänzle, G.J. Nicholson, W.P. Hammes, G. Jung, Angew. Chem. Int. Ed. 39 (2000) 2766–2768.
[9] N.M. Gandhi, J. Nazareth, P.V. Divekar, H. Kohl, N.J. De Souza, J. Antibiot. 26 (1973) 797–798.
[10] D.U. Ganihigama, S. Sureram, S. Sangher, P. Hongmanee, T. Aree, C. Mahidol, S. Ruchirawat, P. Kittakoop, Eur. J. Med. Chem. 89 (2015) 1–12.
[11] X. Mo, Q. Li, J. Ju, RSC Adv. 4 (2014) 50566–50593.
[12] N.U. Sata, S. Matsunaga, N. Fusetani, R.W.M. van Soest, J. Nat. Prod. 62 (1999) 969–971.
[13] R. Kumar, R. Subramani, K.-D. Feussner, W. Aalbersberg, Mar. Drugs 10 (2012)

200–208.
[14] J.Y. Li, G. Strobel, J. Harper, E. Lobkovsky, J. Clardy, Org. Lett. 2 (2000) 767–770.
[15] S. Suzuki, T. Hosoe, K. Nozawa, K. Kawai, T. Yaguchi, S. Udagawa, J. Nat. Prod. 63 (2000) 768–772.
[16] R.E. Schwartz, G.L. Helms, E.A. Bolessa, K.E. Wilson, R.A. Giacobbe, J.S. Tkacz, G.F. Bills, J.M. Liesch, D.L. Zink, J.E. Curotto, B. Pramanik, J.C. Onishi, Tetrahedron 50 (1994) 1675–1686.
[17] Y.-C. Jeong, M. Anwar, Z. Bikadi, E. Hazai, M.G. Moloney, Chem. Sci. 4 (2013) 1008–1015.
[18] L. Josa-Culleré, A. Pretsch, D. Pretsch, M.G. Moloney, J. Org. Chem. 83 (2018) 10303–10317.
[19] T. Rosen, P.B. Fernandes, M.A. Marovich, L. Shen, J. Mao, A.G. Pernet, J. Med. Chem. 32 (1989) 1062–1069.
[20] E.J. Murray, R.C. Crowley, A. Truman, S.R. Clarke, J.A. Cottam, G.P. Jadhav, V.R. Steele, P. O'Shea, C. Lindholm, A. Cockayne, S.R. Chhabra, W.C. Chan, P. Williams, J. Med. Chem. 57 (2014) 2813–2819.
[21] K. Matsuo, I. Kitaguchi, Y. Takata, K. Tanaka, Chem. Pharm. Bull. 28 (1980) 2494–2502.
[22] R. Yendapally, J.G. Hurdle, E.I. Carson, R.B. Lee, R.E. Lee, J. Med. Chem. 51 (2008) 1487–1491.
[23] P.T. Cherian, A. Deshpande, M.N. Cheramie, D.F. Bruhn, J.G. Hurdle, R.E. Lee, J. Antibiot. 70 (2017) 65–72.
[24] P.T. Cherian, M.N. Cheramie, K.R. Marreddy, D.M. Fernando, J.G. Hurdle, R.E. Lee, Bioorg. Med. Chem. Lett. 28 (2018) 3105–3112.
[25] D. Matiadis, O. Igglessi-Markopoulou, Eur. J. Org. Chem. (31) (2010) 5989–5995.
[26] C.A. Mitsos, A.L. Zografos, O. Igglessi-Markopoulou, J. Org. Chem. 65 (2000) 5852–5853.
[27] S. Kikionis, V. McKee, J. Markopoulos, O. Igglessi-Markopoulou, Tetrahedron 65 (2009) 3711–3716.
[28] E. Gavrielatos, C. Mitsos, G. Athanasellis, B.T. Heaton, A. Steiner, J.F. Bickley, O. Igglessi-Markopoulou, J. Markopoulos, J. Chem. Soc. Dalton Trans. (2001) 639–644.
[29] D. Matiadis, O. Igglessi-Markopoulou, V. McKee, J. Markopoulos, Tetrahedron 70 (2014) 2439–2443.
[30] D. Matiadis, D. Tsironis, S. Stefanou, O. Igglessi-Markopoulou, V. McKee, Y. Sanakis, K.N. Lazarou, A. Chrissanthopoulos, S.N. Yannopoulos, J.M. Markopoulos, Bioinorg.Chem. Appl, Article ID 7895023, 10 pages, 2017.
[31] G. Athanasellis, E. Gavrielatos, O. Igglessi-Markopoulou, J. Heterocycl. Chem. 38 (2001) 1203–1208.
[32] M. Petroliagi, O. Igglessi-Markopoulou, J. Chem. Soc. Perkin Trans. 1 (1997) 3543–3548.
[33] R. Muddala, J.A.M. Acosta, L.C.A. Barbosa, J. Boukouvalas, J. Nat. Prod. 80 (2017) 2166–2169.
[34] P. Lv, Y. Chen, Z. Zhao, T. Shi, X. Wu, J. Xue, Q.X. Li, R. Hua, J. Agric. Food Chem. 66 (2018) 1023–1032.
[35] M. Zaghouani, B. Nay, Nat. Prod. Rep. 33 (2016) 540–548.
[36] G. Athanasellis, O. Igglessi-Markopoulou, J. Markopoulos, Bioinorg.Chem. Appl, Article ID 315056, 11 pages, 2010.
[37] M.-H. Lebrun, P. Duvert, F. Gaudemer, A. Gaudemer, C. Deballon, P. Boucly, J. Inorg. Biochem. 24 (1985) 167–181.
[38] B. Biersack, R. Diestel, C. Jagusch, F. Sasse, R. Schobert, J. Inorg. Biochem. 103 (2009) 72–76.
[39] CrysAlis PRO 1.171.38.43, Rigaku Oxford Diffraction, 2015.
[40] C.B. Hübschle, G.M. Sheldrick, B. Dittrich, J. Appl. Crystallogr. 44 (2011) 1281–1284.
[41] G.M. Sheldrick, Acta Cryst A71 (2015) 3–8.
[42] G.M. Sheldrick, Acta Cryst C71 (2015) 3–8.
[43] I.A. Edwards, A.G. Elliott, A.M. Kavanagh, J. Zuegg, M.A.T. Blaskovich, M.A. Cooper, ACS Infect Dis. 2 (2016) 442–450.
[44] M.K. McMillan, L. Li, J.B. Parker, L. Patel, Z. Zhong, J.W. Gunnett, W.J. Powers, M.D. Johnson, Cell Biol. Toxicol. 18 (2002) 157–173.
[45] J. O'Brien, I. Wilson, T. Orton, F. Pognan, Eur. J. Biochem. 267 (2000) 5421–5426.
[46] A.S. Ravipati, S.T. Henriques, A.G. Poth, Q. Kaas, C.K. Wang, M.L. Colgrave, D.J. Craik, ACS Chem. Biol. 10 (2015) 2491–2500.
[47] G.L. Miessler, D.A. Tarr, Inorganic Chemistry (Chapter II), 2nd edition, Prentice Hall, 1999.
[48] C.S. Dilip, V. Thangaraj, A.P. Raj, Arab. J. Chem. 9 (2016) S731–S742.
[49] R.S. Drago, Physical Methods for Chemists, 2nd Edition, Saunders College Publishing, 1992.
[50] V. Reddy, N. Patil, S.D. Angadi, E-J. Chem. 5 (2008) 577–583.
[51] V. Stefanou, D. Matiadis, D. Tsironis, O. Igglessi-Markopoulou, V. McKee, J. Markopoulos, Polyhedron 141 (2018) 289–295.
[52] M.J. Weller, N.A. Young, Cheracterization Methods in Inorganic Chemistry, Oxford University Press, 2017.
[53] J.R. Pilbrow, J. Magn. Res. 31 (1978) 479–490.
[54] Z. Khan, A. Rehman, M.A. Nisar, S. Zafar, S.Z. Hussain, I. Zerr, I. Hussain, M. Waseem, M. Arif, Appl. Microbiol. Biotechnol. 101 (2017) 7715–7728.
[55] S.Z. Abbas, M. Rafatullah, K. Hossain, N. Ismail, H.A. Tajarudin, H.P.S. Abdul Khalil, Int. J. Environ. Sci. Technol. 15 (2018) 243–262.
[56] M.A.T. Blaskovich, J. Zuegg, A.G. Elliott, M.A. Cooper, ACS Infect. Dis. 1 (2015) 285–287.